First Measurement of Energy-Dependent Inclusive Muon Neutrino Charged-Current Cross Sections on Argon with the MicroBooNE Detector

P. Abratenko,[33] R. An,[14] J. Anthony,[4] L. Arellano,[18] J. Asaadi,[32] A. Ashkenazi,[30] S. Balasubramanian,[11] B. Baller,[11] C. Barnes,[20] G. Barr,[23] V. Basque,[18] L. Bathe-Peters,[13] O. Benevides Rodrigues,[29] S. Berkman,[11] A. Bhanderi,[18] A. Bhat,[29] M. Bishai,[2] A. Blake,[16] T. Bolton,[15] J. Y. Book,[13] L. Camilleri,[9] D. Caratelli,[11] I. Caro Terrazas,[8] F. Cavanna,[11] G. Cerati,[11] Y. Chen,[1] D. Cianci,[9] J. M. Conrad,[19] M. Convery,[26] L. Cooper-Troendle,[36] J. I. Crespo-Anadón,[5] M. Del Tutto,[11] S. R. Dennis,[4] P. Detje,[4] A. Devitt,[16] R. Diurba,[21] R. Dorrill,[14] K. Duffy,[11] S. Dytman,[24] B. Eberly,[28] A. Ereditato,[1] J. J. Evans,[18] R. Fine,[17] G. A. Fiorentini Aguirre,[27] R. S. Fitzpatrick,[20] B. T. Fleming,[36] N. Foppiani,[13] D. Franco,[36] A. P. Furmanski,[21] D. Garcia-Gamez,[12] S. Gardiner,[11] G. Ge,[9] S. Gollapinni,[31,17] O. Goodwin,[18] E. Gramellini,[11] P. Green,[18] H. Greenlee,[11] W. Gu,[2] R. Guenette,[13] P. Guzowski,[18] L. Hagaman,[36] O. Hen,[19] C. Hilgenberg,[21] G. A. Horton-Smith,[15] A. Hourlier,[19] R. Itay,[26] C. James,[11] X. Ji,[2] L. Jiang,[34] J. H. Jo,[36] R. A. Johnson,[7] Y.-J. Jwa,[9] D. Kalra,[9] N. Kamp,[19] N. Kaneshige,[3] G. Karagiorgi,[9] W. Ketchum,[11] M. Kirby,[11] T. Kobilarcik,[11] I. Kreslo,[1] I. Lepetic,[25] K. Li,[36] Y. Li,[2] K. Lin,[17] B. R. Littlejohn,[14] W. C. Louis,[17] X. Luo,[3] K. Manivannan,[29] C. Mariani,[34] D. Marsden,[18] J. Marshall,[35] D. A. Martinez Caicedo,[27] K. Mason,[33] A. Mastbaum,[25] N. McConkey,[18] V. Meddage,[15] T. Mettler,[1] K. Miller,[6] J. Mills,[33] K. Mistry,[18] A. Mogan,[31] T. Mohayai,[11] J. Moon,[19] M. Mooney,[8] A. F. Moor,[4] C. D. Moore,[11] L. Mora Lepin,[18] J. Mousseau,[20] M. Murphy,[34] D. Naples,[24] A. Navrer-Agasson,[18] M. Nebot-Guinot,[10] R. K. Neely,[15] D. A. Newmark,[17] J. Nowak,[16] M. Nunes,[29] O. Palamara,[11] V. Paolone,[24] A. Papadopoulou,[19] V. Papavassiliou,[22] S. F. Pate,[22] N. Patel,[16] A. Paudel,[15] Z. Pavlovic,[11] E. Piasetzky,[30] I. D. Ponce-Pinto,[36] S. Prince,[13] X. Qian,[2] J. L. Raaf,[11] V. Radeka,[2] A. Rafique,[15] M. Reggiani-Guzzo,[18] L. Ren,[22] L. C. J. Rice,[24] L. Rochester,[26] J. Rodriguez Rondon,[27] M. Rosenberg,[24] M. Ross-Lonergan,[9] G. Scanavini,[36] D. W. Schmitz,[6] A. Schukraft,[11] W. Seligman,[9] M. H. Shaevitz,[9] R. Sharankova,[33] J. Shi,[4] J. Sinclair,[1] A. Smith,[4] E. L. Snider,[11] M. Soderberg,[29] S. Söldner-Rembold,[18] P. Spentzouris,[11] J. Spitz,[20] M. Stancari,[11] J. St. John,[11] T. Strauss,[11] K. Sutton,[9] S. Sword-Fehlberg,[22] A. M. Szelc,[10] W. Tang,[31] K. Terao,[26] C. Thorpe,[16] D. Totani,[3] M. Toups,[11] Y.-T. Tsai,[26] M. A. Uchida,[4] T. Usher,[26] W. Van De Pontseele,[23,13] B. Viren,[2] M. Weber,[1] H. Wei,[2] Z. Williams,[32] S. Wolbers,[11] T. Wongjirad,[33] M. Wospakrik,[11] K. Wresilo,[4] N. Wright,[19] W. Wu,[11] E. Yandel,[3] T. Yang,[11] G. Yarbrough,[31] L. E. Yates,[19] H. W. Yu,[2] G. P. Zeller,[11] J. Zennamo,[11] and C. Zhang[2]

(MicroBooNE Collaboration)[*]

[1]*Universität Bern, Bern CH-3012, Switzerland*
[2]*Brookhaven National Laboratory (BNL), Upton, New York 11973, USA*
[3]*University of California, Santa Barbara, California 93106, USA*
[4]*University of Cambridge, Cambridge CB3 0HE, United Kingdom*
[5]*Centro de Investigaciones Energéticas, Medioambientales y Tecnológicas (CIEMAT), Madrid E-28040, Spain*
[6]*University of Chicago, Chicago, Illinois 60637, USA*
[7]*University of Cincinnati, Cincinnati, Ohio 45221, USA*
[8]*Colorado State University, Fort Collins, Colorado 80523, USA*
[9]*Columbia University, New York, New York 10027, USA*
[10]*University of Edinburgh, Edinburgh EH9 3FD, United Kingdom*
[11]*Fermi National Accelerator Laboratory (FNAL), Batavia, Illinois 60510, USA*
[12]*Universidad de Granada, Granada E-18071, Spain*
[13]*Harvard University, Cambridge, Massachusetts 02138, USA*
[14]*Illinois Institute of Technology (IIT), Chicago, Illinois 60616, USA*
[15]*Kansas State University (KSU), Manhattan, Kansas 66506, USA*
[16]*Lancaster University, Lancaster LA1 4YW, United Kingdom*
[17]*Los Alamos National Laboratory (LANL), Los Alamos, New Mexico 87545, USA*
[18]*The University of Manchester, Manchester M13 9PL, United Kingdom*
[19]*Massachusetts Institute of Technology (MIT), Cambridge, Massachusetts 02139, USA*
[20]*University of Michigan, Ann Arbor, Michigan 48109, USA*
[21]*University of Minnesota, Minneapolis, Minnesota 55455, USA*
[22]*New Mexico State University (NMSU), Las Cruces, New Mexico 88003, USA*
[23]*University of Oxford, Oxford OX1 3RH, United Kingdom*
[24]*University of Pittsburgh, Pittsburgh, Pennsylvania 15260, USA*

[25]Rutgers University, Piscataway, New Jersey 08854, USA
[26]SLAC National Accelerator Laboratory, Menlo Park, California 94025, USA
[27]South Dakota School of Mines and Technology (SDSMT), Rapid City, South Dakota 57701, USA
[28]University of Southern Maine, Portland, Maine 04104, USA
[29]Syracuse University, Syracuse, New York 13244, USA
[30]Tel Aviv University, Tel Aviv 69978, Israel
[31]University of Tennessee, Knoxville, Tennessee 37996, USA
[32]University of Texas, Arlington, Texas 76019, USA
[33]Tufts University, Medford, Massachusetts 02155, USA
[34]Center for Neutrino Physics, Virginia Tech, Blacksburg, Virginia 24061, USA
[35]University of Warwick, Coventry CV4 7AL, United Kingdom
[36]Department of Physics, Wright Laboratory, Yale University, New Haven, Connecticut 06520, USA

(Received 31 October 2021; accepted 9 March 2022; published 12 April 2022)

We report a measurement of the energy-dependent total charged-current cross section $\sigma(E_\nu)$ for inclusive muon neutrinos scattering on argon, as well as measurements of flux-averaged differential cross sections as a function of muon energy and hadronic energy transfer (ν). Data corresponding to 5.3×10^{19} protons on target of exposure were collected using the MicroBooNE liquid argon time projection chamber located in the Fermilab booster neutrino beam with a mean neutrino energy of approximately 0.8 GeV. The mapping between the true neutrino energy E_ν and reconstructed neutrino energy E_ν^{rec} and between the energy transfer ν and reconstructed hadronic energy $E_{\mathrm{had}}^{\mathrm{rec}}$ are validated by comparing the data and Monte Carlo (MC) predictions. In particular, the modeling of the missing hadronic energy and its associated uncertainties are verified by a new method that compares the $E_{\mathrm{had}}^{\mathrm{rec}}$ distributions between data and a MC prediction after constraining the reconstructed muon kinematic distributions, energy, and polar angle to those of data. The success of this validation gives confidence that the missing energy in the MicroBooNE detector is well modeled and underpins first-time measurements of both the total cross section $\sigma(E_\nu)$ and the differential cross section $d\sigma/d\nu$ on argon.

DOI: 10.1103/PhysRevLett.128.151801

Current and next-generation precision neutrino oscillation experiments aim to answer several critical questions in particle physics [1] by (i) searching for CP violation in the lepton sector [2,3], (ii) determining the neutrino mass ordering [4], and (iii) searching for light sterile neutrinos [5]. For this purpose, the short-baseline neutrino program [6] and the deep underground neutrino experiment [7,8] employ liquid argon time projection chambers (LArTPCs) [9–12], a tracking calorimeter that enables excellent neutrino flavor identification and neutrino energy (E_ν) reconstruction in the GeV energy range [13]. These experiments are designed to measure the neutrino flavor oscillations as a function of E_ν, which requires a good understanding of the neutrino energy spectrum, neutrino-argon interaction cross sections [14], and LArTPC detector response. High-precision measurements of ν-Ar cross sections, particularly those related to energy reconstruction, are of paramount importance.

While historical accelerator-based neutrino experiments often reported E_ν-dependent cross sections [15,16], recent experiments tend to limit cross section measurements to the directly observable lepton and/or hadron kinematics [17]. This paradigm shift was triggered by concerns that quantities not directly measurable in detectors (e.g., the missing hadronic energy of the interaction from undetected neutral particles) may not be correctly modeled in simulations, which is of particular concern in a broadband neutrino beam. In this Letter, we demonstrate that the MicroBooNE tune model [18] (based on GENIE-v3 [19]) of missing energy with its associated uncertainty can be validated with inclusive muon neutrino charged-current (ν_μCC) interactions from the MicroBooNE detector [20]. After constraining the lepton kinematics distributions of Monte Carlo (MC) prediction to those of data, the comparison of reconstructed hadronic energy $E_{\mathrm{had}}^{\mathrm{rec}}$ distributions between data and the updated MC prediction reveals whether the model is able to describe the relationship between the lepton kinematics and the visible hadronic energy. This procedure validates whether the missing hadronic energy is sufficiently modeled given the prior knowledge of the neutrino flux and detector effects. This new procedure enables a first measurement of the differential cross section as a function of the energy transfer to the argon $d\sigma/d\nu$. Together with the differential cross section as a function of the muon energy ($d\sigma/dE_\mu$), the E_ν-dependent cross

sections are extracted. These data could be used to isolate problems for low-E_ν cross sections and to reduce modeling uncertainties for the low-ν method [21–23] to constrain the shape of neutrino energy spectrum in future experiments.

The MicroBooNE detector is a $10.4 \times 2.6 \times 2.3$ m^3 LArTPC. It consists of approximately 85 ton of liquid Ar in the active time projection chamber (TPC) volume for ionization charge detection, along with 32 photomultiplier tubes (PMTs) [24] for scintillation light detection. This Letter makes use of a dataset corresponding to an exposure of 5.3×10^{19} protons on target (POT) from the booster neutrino beamline (BNB), which produces a neutrino flux with an estimated 93.6% ν_μ purity [25] and a mean E_ν of 0.8 GeV. At these energies, ν-Ar interactions are dominated by quasielastic and meson-exchange current interactions as well as resonant pion productions, and the final-state hadrons consist mostly of protons and neutrons with some charged and neutral pions. The $\mathcal{O}(1)$ MeV energy threshold [26] of LArTPC allows detecting these particles down to low kinetic energies.

Compared to earlier work [27], this measurement incorporates an improved TPC detector simulation and signal processing procedure [28,29], the Wire-Cell tomographic event reconstruction [30,31], and a many-to-many TPC-charge to PMT-light matching algorithm for cosmic-ray rejection [31]. In particular, the "generic neutrino detection" [32,33], which limits the cosmic-ray muon backgrounds to below 15% at over 80% ν_μCC selection efficiency, is used as a preselection. The ν_μCC event selection is further improved using a set of pattern recognition techniques, including (i) neutrino vertex identification, (ii) track and shower topology separation, (iii) particle identification, and (iv) particle flow reconstruction in the Wire-Cell reconstruction package [34]. Since many of the analysis details in this Letter, including the event reconstruction, event selection, overall model prediction along with its systematic uncertainties, and the model validation, are in common with those in searching for an anomalous low-energy excess in an inclusive charged-current ν_e channel that was documented in Ref. [35], they are only briefly reviewed in this Letter.

First, the reconstructed neutrino vertex is required to be inside a fiducial volume, defined to be 3 cm inside the effective detector boundary [33]. Second, a set of dedicated background taggers are constructed to further reject residual muon backgrounds that entered the detector from outside based on directional information. Finally, neutral-current (NC) events are substantially reduced by requiring a reconstructed primary muon candidate to be longer than 5 cm. Some limited charged pion rejection is achieved by detecting large-angle scattering in reconstructed track trajectories. Using input variables from the background taggers, a multivariate classifier is constructed using the modern boosted decision tree library XGBoost [36] that yields a ν_μCC selection with an estimated 92% purity and 68% efficiency [35]. In total, 11 528 ν_μCC candidates are selected and used for cross section extraction. About $1/3$ of the events are fully contained (FC) and $2/3$ are partially contained (PC). Here, the FC events are defined to be events with their main TPC cluster [31] fully contained within the fiducial volume [33] and PC events are mostly because of exiting muons.

Three methods are used to reconstruct the energy of tracks and electromagnetic (EM) showers [34,35]: (i) The energy of a stopped charged particle track can be estimated by its travel *range* using the NIST PSTAR database [37]. (ii) The kinetic energy of a charged particle track can be estimated by integrating over the reconstructed energy loss per unit length dE/dx, which is calculated from the measured dQ/dx (ionization charge per unit length) using a *recombination* model [38]. (iii) The energy of an EM shower can be estimated calorimetrically by *scaling* the total reconstructed charge of the EM shower with a factor of 2.50, which is derived from simulation and includes the bias in the reconstructed charge [31] and the average recombination factor. This factor is validated with the reconstructed invariant mass of the neutral pion [39]. For stopping tracks with trajectories longer than 4 cm, the range method is used to estimate the energy. For short tracks (< 4 cm), tracks exiting the detector, tracks with "wiggled" topology [34] (e.g., low-energy electrons), and muon tracks with identified δ rays, the recombination method is used to estimate its kinetic energy.

The reconstructed neutrino energy E_ν^{rec} per event is estimated by summing the kinetic energies of each reconstructed (visible) final-state particle. For each reconstructed muon, charged pion, or electron candidate, its mass is added to the energy reconstruction. An average binding energy of 8.6 MeV [40] was added for each proton identified. Figure 1 shows the FC ν_μCC distribution as a function of reconstructed neutrino energy, the selection efficiency as a function of true neutrino energy, and the smearing matrix between E_ν^{rec} and E_ν according to the Monte Carlo simulation. The predicted energy resolution using the MicroBooNE MC simulation for FC ν_μCC events is ~10% for muon energy, ~20% for neutrino energy, and ~30%–50% for hadronic energy. The hadronic energy resolution is dominated by the missing hadronic energy and imperfect event reconstruction. For events well reconstructed, the resolution of the reconstructed visible hadronic energy approaches ~10%. Among all events, the average bias (toward low energy) of E_ν^{rec} for FC ν_μCC events is less than 10% for $E_\nu < 800$ MeV and increases to ~25% at $E_\nu = 2.5$ GeV.

The total and differential cross sections are extracted using the Wiener–singular value decomposition (SVD) unfolding method [41] as follows:

$$M_i - B_i = \sum_j R_{ij} S_j = \sum_j \tilde{\Delta}_{ij} \tilde{F}_j S_j. \tag{1}$$

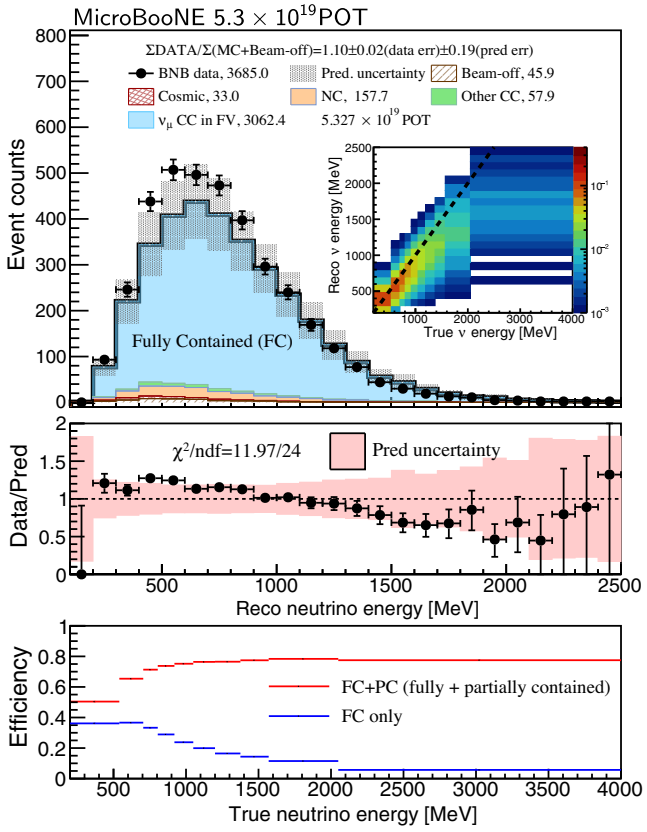

FIG. 1. Top: distribution of the selected FC ν_μCC events as a function of reconstructed neutrino energy. Inset: the smearing matrix from true neutrino energy to reconstructed neutrino energy. Middle: data-prediction ratio. The pink band represents the total uncertainty (statistical and systematic) of the MC prediction. Bottom: selection efficiency of the ν_μCC events in the fiducial volume as a function of true neutrino energy. At high neutrino energy, muons are more likely to exit the TPC, which leads an increase (decrease) in the efficiency of PC (FC) samples.

M_i is the measured number of events in bin i of the reconstructed energy space, and B_i is the expected number of backgrounds. $R_{ij} = \tilde{\Delta}_{ij}\tilde{F}_j$ is the overall response matrix. S_j, to be extracted, is the average (differential) cross section in bin j of the true energy, weighted by the nominal ν_μ neutrino flux, which is tabulated in Ref. [27]. This definition of S_j with the nominal neutrino flux coincides with a recommendation from Ref. [42] in addressing a concern on the treatment of neutrino flux uncertainty. $\tilde{\Delta}_{ij}$, the ratio between the selected number of events in reconstructed energy bin i that originate from the true energy bin j and the generated number of events in bin j, is calculated using central value MC. This encapsulates both the smearing between reconstructed and true space and the efficiency. $\tilde{F}_j$ is a constant that is calculated with the POT, number of Ar nuclei, the integrated nominal ν_μ flux in bin j, and the bin width (for differential cross sections only).

The Wiener-SVD unfolding is performed based on a

$$\chi^2 = (\boldsymbol{M} - \boldsymbol{B} - \boldsymbol{R}\cdot\boldsymbol{S})^T \cdot \boldsymbol{V}^{-1} \cdot (\boldsymbol{M} - \boldsymbol{B} - \boldsymbol{R}\cdot\boldsymbol{S}) \quad (2)$$

test statistics and an additional regularization constructed from a Wiener filter [41]. $\boldsymbol{V}$ is the covariance matrix on the measured number of events in the reconstructed energy bins, encoding the statistical and systematic uncertainties for both signal and background events. Statistical uncertainties on the data are calculated following the combined Neyman-Pearson procedure [43].

The covariance matrix also includes several systematic uncertainties. The neutrino flux model uncertainty (5%–15%) follows the work in Ref. [27]. It includes effects from hadron production of π^+, π^-, K^+, K^-, and K^0_L, together with total, inelastic, and quasielastic cross sections of pion and nucleon rescattering on beryllium and aluminum. In addition, modeling of the horn current distribution and calibration is included. The neutrino-argon interaction cross section model uncertainties (∼20%) are described in Ref. [18]. Particularly, the uncertainties associated with the hadronic interactions, which are important in modeling missing energy, are conservatively estimated: the proton to neutron charge exchange and the proton knockout have 50% and 20% uncertainties, respectively [44,45]. The uncertainties on the GEANT4 models [46] used to simulate secondary interactions of protons and charged pions outside the target nucleus (∼1.5%) follows Ref. [47]. These uncertainties on the flux, cross section, and GEANT4 models are estimated using a *multisim* technique [48] in which parameters that govern interaction models are simultaneously varied in generating hundreds of universes to construct covariance matrices.

The detector response uncertainty follows the work in Ref. [49], considering the effects of variations in the TPC waveform, light yield and propagation, space charge effect [50,51], and ionization recombination model. For each source, the same set of MC interactions are resimulated through the detector response simulation with a 1σ change to the corresponding detector model parameter. The differences in the selected number of events between the modified and original simulations are used to construct a covariance matrix with a bootstrapping [52] procedure. The uncertainty of modeling the "dirt" events that originate outside the cryostat follows the work in Ref. [35]. The statistical uncertainty of the Monte Carlo sample is treated using the methods described in Ref. [53]. The uncertainties on the POT (2% based on *in situ* proton flux measurements [25]) and the number of target nuclei (∼1%) are also included.

Given Eq. (1), the uncertainties on the neutrino flux, GEANT4 model, detector model, and POT enter through B_i and the numerator of $\tilde{\Delta}_{ij}$. Dirt uncertainties enter through B_i. In comparison, the cross section uncertainty enters through B_i and both numerator and denominator of $\tilde{\Delta}_{ij}$. Although the uncertainty on the predicted inclusive cross

section is ∼20%, it is reduced to ∼5% because of the cancellation between numerator and denominator of $\tilde{\Delta}_{ij}$.

A prior condition of using the Wiener-SVD unfolding method to extract cross sections is that the data must be well described by the overall model prediction within its uncertainties. In Figs. 1 and 2, data and simulation are shown for key reconstructed kinematic variables including (i) neutrino energy $E_\nu^{\rm rec}$, (ii) muon energy $E_\mu^{\rm rec}$, (iii) cosine of muon polar angle $\cos\theta_\mu^{\rm rec}$, and (iv) hadronic energy $E_{\rm had}^{\rm rec}$. The compatibility between the data and prediction is demonstrated quantitatively by decent χ^2/NDF values (NDF is the number of degrees of freedom) with corresponding p values larger than 0.05 considering full uncertainties using the Pearson χ^2 [54]. To examine different components of systematic uncertainties, we further utilize the conditional covariance matrix formalism [55] to adjust the model prediction and reduce its uncertainties by applying constraints from data. Figure 2(a) shows the comparison of the $E_\mu^{\rm rec}$ distribution for PC ν_μCC in data to that of the model prediction after applying constraints from the FC $E_\mu^{\rm rec}$ events. While the uncertainties are largely reduced, there is only a small change to χ^2/NDF. The data and constrained model agree within uncertainties, verifying the modeling of the invisible energy of muons outside the active detector volume for PC events. Figure 2(b) shows the comparison of the $\cos\theta_\mu^{\rm rec}$ distribution for both FC and PC ν_μCC candidates in data with the model prediction after applying a constraint from the $E_\mu^{\rm rec}$ distributions of the same set of ν_μCC candidate events. Compared to the previous case, the correlated statistical uncertainties between the $\cos\theta_\mu^{\rm rec}$ distributions and the $E_\mu^{\rm rec}$ distributions are estimated with a bootstrapping procedure. While the uncertainties are significantly reduced after applying the constraint, the change to χ^2/NDF is small, showing well-modeled muon kinematics.

We will examine the modeling of the mapping between the reconstructed energy of the hadronic system $E_{\rm had}^{\rm rec}$ and the energy transfer to the argon nucleus $\nu = E_\nu - E_\mu$ after taking into account the muon results. The mapping of $E_{\rm had}^{\rm rec}$ to ν (or $E_\nu^{\rm rec}$ to true E_ν) relies on the overall cross section model to correct for the missing energy going into undetected neutrons, low-energy photons, and other particles below the detection threshold. To validate the model, we examine the $E_{\rm had}^{\rm rec}$ distribution for the FC ν_μCC candidates in data with that of the model prediction after applying constraints from two one-dimensional distributions in muon kinematics: $E_\mu^{\rm rec}$ and $\cos\theta_\mu^{\rm rec}$ in Fig. 2(c). After applying constraints, the uncertainties on the model prediction for $E_{\rm had}^{\rm rec}$ are significantly reduced because of the cancellation of common systematic uncertainties, such as neutrino flux. At the lowest energies, it reduces from 20% to 5%. Nevertheless, the χ^2/NDF values still yields p value above 0.5, indicating that the model describes the relationship between $E_{\rm had}^{\rm rec}$ and $E_\mu^{\rm rec}$ well within its uncertainty.

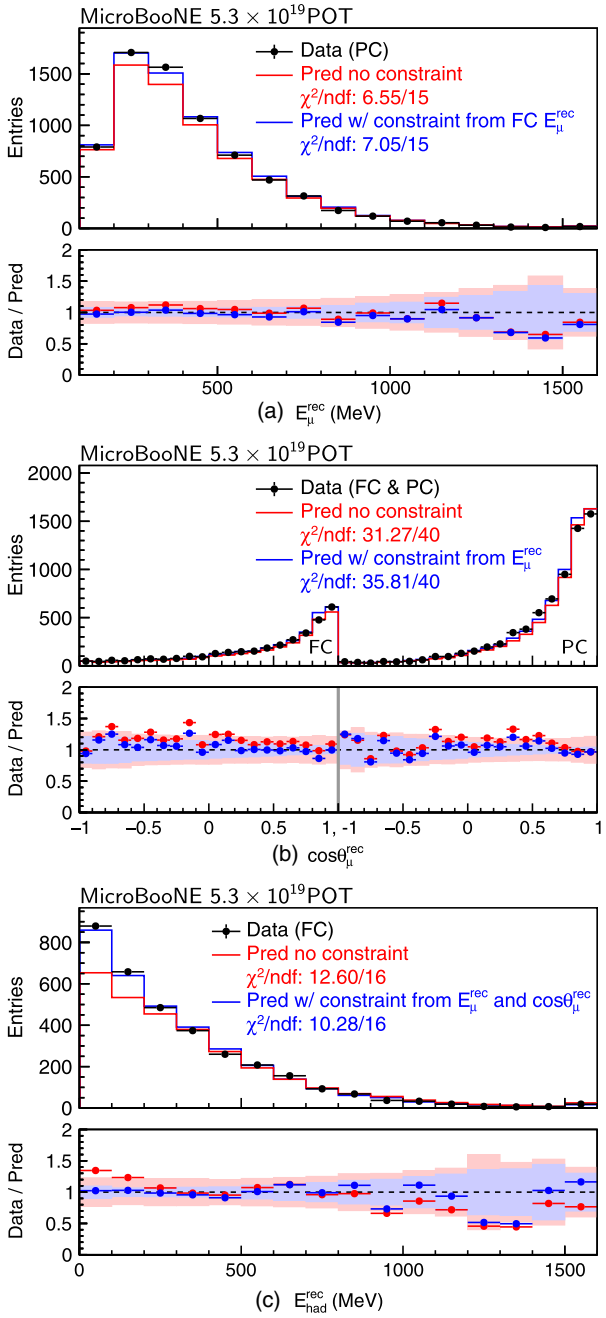

FIG. 2. Data are compared with MC predictions as a function of (a) reconstructed muon energy $E_\mu^{\rm rec}$ for the partially contained (PC) sample. The MC prediction after applying constraints from the fully contained sample in $E_\mu^{\rm rec}$ is shown. The last bin represents all events with $E_\mu^{\rm rec} > 1.5$ GeV. The blue (red) points represent the ratio between data and the MC prediction with (without) constraint, and the bands with same colors depict the total (include statistical) uncertainty of the MC prediction. (b) reconstructed $\cos\theta_\mu^{\rm rec}$ for the FC (first half) and PC (second half) sample. The MC prediction after applying constraints on both FC and PC samples in $E_\mu^{\rm rec}$ is shown. (c) reconstructed hadronic energy $E_{\rm had}^{\rm rec}$ for the FC sample. The MC prediction after applying constraints on muon kinematics ($E_\mu^{\rm rec}$ and $\cos\theta_\mu^{\rm rec}$) is shown. The last bin represents all events with $E_{\rm had}^{\rm rec} > 1.5$ GeV.

In particular, the difference between the data and the model prediction in the first three bins of $E_{\mathrm{had}}^{\mathrm{rec}}$ is significantly reduced after applying the constraints. This test further validates that the modeling of the missing hadronic energy can describe data within its associated uncertainty. We note the conditional covariance matrix formalism, which is used to update the MC predictions and their uncertainties given the data constraints (more details can be found in Ref. [35]), is only used in validating the overall model and is not used in extracting cross sections through the unfolding procedure. With fake data, we show that the χ^2/NDF has a significant increase with a shift of ∼15% in the hadronic energy fraction allocated to protons (mimicking a variation of the proton-inelastic cross section), and this procedure is also able to distinguish between two GENIE models (see Supplemental Material [56]). In addition, the model validation procedure is shown to be much more sensitive to detect an insufficient input model compared to the extracted cross sections.

With the overall model validated, the total and differential cross sections per nucleon are extracted. The binning of the unfolded results is chosen by considering the energy resolution and the number of samples in the true space. Considering both FC and PC samples, the total cross section divided by the bin-center neutrino energy is shown as a function of neutrino energy in Fig. 3(a), where the bin center is calculated as the flux-weighted average neutrino energy. Excluding the PC sample does not change the overall behavior of the cross sections, but increases their uncertainties for neutrino energy above 1.2 GeV modestly. Besides the nominal cross section model used in the "MicroBooNE MC" [18], predictions from GENIE v3.0.6 [19,44], NuWro 19.02.01 [77], NEUT 5.4.0.1 [78], and GiBUU 2019.08 [79] after applying the Wiener filter are quantitatively compared with the measurement through calculating χ^2/NDF with the uncertainty covariance matrix obtained from the unfolding procedure. Note that these comparisons only incorporate the central predictions from various generators without their theoretical uncertainties, which are particularly important in constructing predictions in analysis. The central predictions of GENIE v3 and NuWro are disfavored compared to the other three. Particularly, the MicroBooNE MC (tuned GENIE-v3 model [18]) has better agreement than GENIE v3.0.6, given the tuned GENIE-v3 model is constructed by fitting T2K data [80] in a similar energy range.

Figures 3(b) and 3(c) show the flux-averaged differential cross sections as a function of muon energy ($d\sigma/dE_\mu$) and energy transfer to the argon nucleus ($d\sigma/d\nu$). The same set of model predictions are compared to these measurements. The model comparison of $d\sigma/dE_\mu$ shows a shape agreement with most models, although the normalization predictions differ. The central predictions of GENIE v3 and NuWro are more disfavored. The model predictions in $d\sigma/d\nu$ show large variations, particularly in the low-energy transfer (ν) region, where the shape difference contributes considerably to the χ^2/NDF given the correlations in the uncertainty covariance matrix. The central prediction from GiBUU has the best agreement with data in the low-ν region, but is systematically lower than data at the high-ν region, which could be originated from an underestimation of the cross sections in the nucleon resonance region beyond Δ. Considering all three cross section results, the GiBUU prediction has the best agreement with acceptable χ^2/NDF values, while the performance of the NEUT prediction is comparable. The central predictions of the other three models show larger disagreement.

In summary, we present a measurement of cross section as a function of the neutrino energy based on data from a broadband neutrino beam. We report the

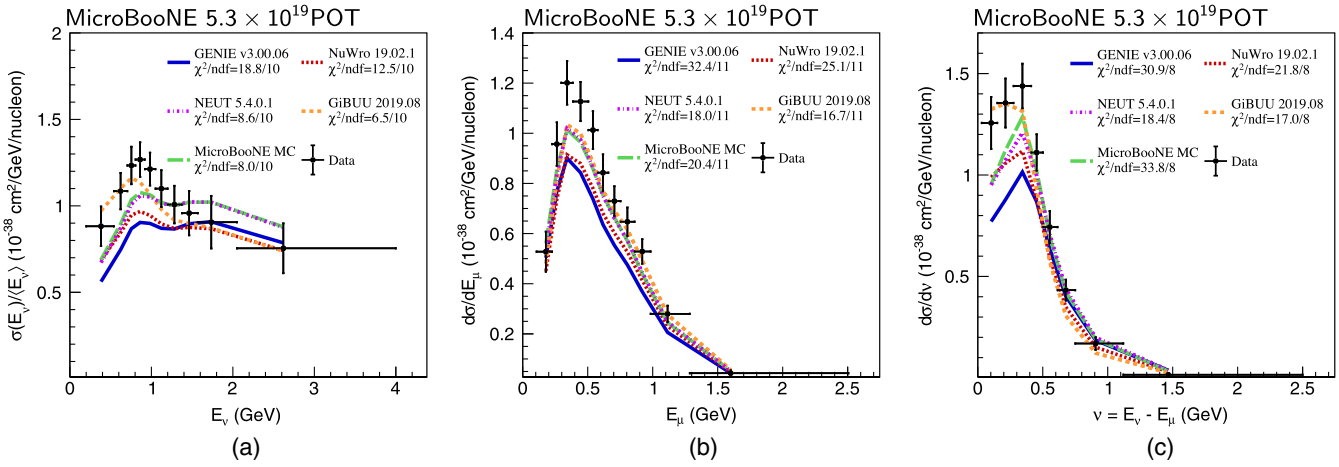

FIG. 3. (a) The extracted ν_μCC inclusive scattering cross section per nucleon divided by the bin-center neutrino energy, as a function of neutrino energy. (b) The measured ν_μCC differential cross section per nucleon as a function of muon energy $d\sigma/dE_\mu$. (c) The measured ν_μCC differential cross section per nucleon as a function of energy transfer $d\sigma/d\nu$. Various model predictions are compared to all three measurements (see text for details).

nominal-flux-weighted total inclusive ν_μCC cross sections $\sigma(E_\nu)$ and the nominal-flux-averaged differential cross sections as a function of muon energy $d\sigma/dE_\mu$ and energy transfer $d\sigma/d\nu$ using the Wiener-SVD unfolding method [41]. A new procedure based on the conditional covariance matrix formalism [55] and the bootstrapping method [52] is used to validate the model of missing energies, which enables the first measurement of $d\sigma/d\nu$ on argon and significantly adds value to the measurement of the total cross section as function of neutrino energy $\sigma(E_\nu)$. These results provide a detailed way to compare data and calculations beyond what is possible with existing flux-averaged total cross section results. With additional accumulated data statistics (up to 1.2×10^{21} POT from BNB) in the MicroBooNE detector, additional neutrino cross section measurements are expected that will lead to further model development and generator improvements for neutrino scattering in argon.

This document was prepared by the MicroBooNE Collaboration using the resources of the Fermi National Accelerator Laboratory (Fermilab), a U.S. Department of Energy, Office of Science, HEP User Facility. Fermilab is managed by Fermi Research Alliance, LLC (FRA), acting under Contract No. DE-AC02-07CH11359. MicroBooNE is supported by the following: the U.S. Department of Energy, Office of Science, Offices of High Energy Physics and Nuclear Physics; the U.S. National Science Foundation; the Swiss National Science Foundation; the Science and Technology Facilities Council (STFC), part of the United Kingdom Research and Innovation; the Royal Society (United Kingdom); and the European Union's Horizon 2020 Marie Sklodowska-Curie Actions. Additional support for the laser calibration system and cosmic ray tagger was provided by the Albert Einstein Center for Fundamental Physics, Bern, Switzerland. We also acknowledge the contributions of technical and scientific staff to the design, construction, and operation of the MicroBooNE detector as well as the contributions of past collaborators to the development of MicroBooNE analyses, without whom this work would not have been possible.

*microboone_info@fnal.gov

[1] M. V. Diwan, V. Galymov, X. Qian, and A. Rubbia, Long-baseline neutrino experiments, Annu. Rev. Nucl. Part. Sci. **66**, 47 (2016).

[2] K. Abe *et al.* (T2K Collaboration), Improved constraints on neutrino mixing from the T2K experiment with 3.13×10^{21} protons on target, Phys. Rev. D **103**, 112008 (2021).

[3] M. A. Acero *et al.* (NOvA Collaboration), An improved measurement of neutrino oscillation parameters by the NOνA experiment, arXiv:2108.08219.

[4] X. Qian and P. Vogel, Neutrino mass hierarchy, Prog. Part. Nucl. Phys. **83**, 1 (2015).

[5] P. A. Machado, O. Palamara, and D. W. Schmitz, The short-baseline neutrino program at Fermilab, Annu. Rev. Nucl. Part. Sci. **69**, 363 (2019).

[6] M. Antonello *et al.* (MicroBooNE, LAr1-ND, ICARUS-WA104 Collaborations), A proposal for a three detector short-baseline neutrino oscillation program in the Fermilab booster neutrino beam, arXiv:1503.01520.

[7] R. Acciarri *et al.* (DUNE Collaboration), Long-Baseline Neutrino Facility (LBNF) and Deep Underground Neutrino Experiment (DUNE), arXiv:1601.05471.

[8] B. Abi *et al.* (DUNE Collaboration), Deep underground neutrino experiment (DUNE), far detector technical design report, volume I introduction to DUNE, J. Instrum. **15**, T08008 (2020).

[9] C. Rubbia, The liquid argon time projection chamber: A new concept for neutrino detectors, Reports No. CERN-EP-INT-77-08, CERN-EP-77-08, 1977, http://cds.cern.ch/record/117852/.

[10] H. H. Chen, P. E. Condon, B. C. Barish, and F. J. Sciulli, A neutrino detector sensitive to rare processes. I. A study of neutrino electron reactions, Report No. FERMILAB-PROPOSAL-0496, 1976, https://inspirehep.net/files/df1edf05d33a55edbb411bdebb802f58.

[11] W. Willis and V. Radeka, Liquid argon ionization chambers as total absorption detectors, Nucl. Instrum. Methods **120**, 221 (1974).

[12] D. Nygren, The time projection chamber: A new 4 pi detector for charged particles, eConf **C740805**, 58 (1974), https://lss.fnal.gov/conf/C740805/p58.pdf.

[13] F. Cavanna, A. Ereditato, and B. T. Fleming, Advances in liquid argon detectors, Nucl. Instrum. Methods Phys. Res., Sect. A **907**, 1 (2018).

[14] J. A. Formaggio and G. P. Zeller, From eV to EeV: Neutrino cross sections across energy scales, Rev. Mod. Phys. **84**, 1307 (2012).

[15] P. Adamson *et al.* (MINOS Collaboration), Neutrino and antineutrino inclusive charged-current cross section measurements with the MINOS near detector, Phys. Rev. D **81**, 072002 (2010).

[16] A. A. Aguilar-Arevalo *et al.* (MiniBooNE Collaboration), Measurement of neutrino-induced charged-current charged pion production cross sections on mineral oil at $E_\nu \sim 1$ GeV, Phys. Rev. D **83**, 052007 (2011).

[17] P. A. Zyla *et al.* (Particle Data Group), Review of particle physics (Section 51), Prog. Theor. Exp. Phys. **2020**, 083C01 (2020).

[18] P. Abratenko *et al.* (MicroBooNE Collaboration), New theory-driven GENIE tune for MicroBooNE, arXiv:2110.14028 [Phys. Rev. D (to be published)].

[19] L. Alvarez-Ruso *et al.* (GENIE Collaboration), Recent highlights from GENIE v3, Eur. Phys. J. Special Topics **230**, 4449 (2021).

[20] R. Acciarri *et al.* (MicroBooNE Collaboration), Design and construction of the MicroBooNE detector, J. Instrum. **12**, P02017 (2017).

[21] S. R. Mishra, in *Proceedings of the Workshop on Hadron Structure Functions and Parton Distributions*, edited by D. Geesaman *et al.* (World Scientific Pub Co Inc., 1991).

[22] W. Seligman, Ph.D. thesis, Columbia University, 1997.

[23] A. Bodek, U. Sarica, D. Naples, and L. Ren, Methods to determine neutrino flux at low energies: Investigation of the low ν method, Eur. Phys. J. C **72**, 1973 (2012).

[24] J. Conrad, B. J. P. Jones, Z. Moss, T. Strauss, and M. Toups, The photomultiplier tube calibration system of the MicroBooNE experiment, J. Instrum. **10**, T06001 (2015).

[25] A. A. Aguilar-Arevalo *et al.* (MiniBooNE Collaboration), The neutrino flux prediction at MiniBooNE, Phys. Rev. D **79**, 072002 (2009).

[26] R. Acciarri *et al.* (ArgoNeuT Collaboration), Demonstration of MeV-scale physics in liquid argon time projection chambers using ArgoNeuT, Phys. Rev. D **99**, 012002 (2019).

[27] P. Abratenko *et al.* (MicroBooNE Collaboration), First Measurement of Inclusive Muon Neutrino Charged Current Differential Cross Sections on Argon at $E_\nu \sim 0.8$ GeV with the MicroBooNE Detector, Phys. Rev. Lett. **123**, 131801 (2019).

[28] C. Adams *et al.* (MicroBooNE Collaboration), Ionization electron signal processing in single phase LArTPCs. Part I. Algorithm description and quantitative evaluation with MicroBooNE simulation, J. Instrum. **13**, P07006 (2018).

[29] C. Adams *et al.* (MicroBooNE Collaboration), Ionization electron signal processing in single phase LArTPCs. Part II. Data/simulation comparison and performance in MicroBooNE, J. Instrum. **13**, P07007 (2018).

[30] X. Qian, C. Zhang, B. Viren, and M. Diwan, Three-dimensional imaging for large LArTPCs, J. Instrum. **13**, P05032 (2018).

[31] P. Abratenko *et al.* (MicroBooNE Collaboration), Neutrino event selection in the MicroBooNE liquid argon time projection chamber using Wire-Cell 3D imaging, clustering, and charge-light matching, J. Instrum. **16**, P06043 (2021).

[32] P. Abratenko *et al.* (MicroBooNE Collaboration), High-performance generic neutrino detection in a LArTPC near the Earth's surface with the MicroBooNE detector, arXiv:2012.07928.

[33] P. Abratenko *et al.* (MicroBooNE Collaboration), Cosmic Ray Background Rejection with Wire-Cell LArTPC Event Reconstruction in the MicroBooNE Detector, Phys. Rev. Applied **15**, 064071 (2021).

[34] P. Abratenko *et al.* (MicroBooNE Collaboration), Wire-cell 3D pattern recognition techniques for neutrino event reconstruction in large LArTPCs: Algorithm description and quantitative evaluation with MicroBooNE simulation, J. Instrum. **17**, P01037 (2022).

[35] P. Abratenko *et al.* (MicroBooNE Collaboration), Search for an anomalous excess of inclusive charged-current ν_e interactions in the MicroBooNE experiment using Wire-Cell reconstruction, arXiv:2110.13978.

[36] T. Chen and C. Guestrin, XGBoost: A scalable tree boosting system, arXiv:1603.02754.

[37] PSTAR at NIST: https://physics.nist.gov/PhysRefData/Star/Text/PSTAR.html.

[38] C. Adams *et al.* (MicroBooNE Collaboration), Calibration of the charge and energy response of the MicroBooNE liquid argon time projection chamber using muons and protons, J. Instrum. **15**, P03022 (2020).

[39] C. Adams *et al.* (MicroBooNE Collaboration), Reconstruction and measurement of $\mathcal{O}(100)$ MeV energy electromagnetic activity from $\pi^0 \to \gamma\gamma$ decays in the MicroBooNE LArTPC, J. Instrum. **15**, P02007 (2020).

[40] S. Sukhoruchkin and Z. Soroko, Atomic mass and nuclear binding energy for ar-40 (argon), *Nuclei with z=1–54*, Landolt-Börnstein–Group I Elementary Particles, Nuclei and Atoms (Springer-Verlag, Berlin Heidelberg, 2009), Vol. 22a, 10.1007/978-3-540-69945-3_558.

[41] W. Tang, X. Li, X. Qian, H. Wei, and C. Zhang, Data unfolding with Wiener-SVD method, J. Instrum. **12**, P10002 (2017).

[42] L. Koch and S. Dolan, Treatment of flux shape uncertainties in unfolded, flux-averaged neutrino cross-section measurements, Phys. Rev. D **102**, 113012 (2020).

[43] X. Ji, W. Gu, X. Qian, H. Wei, and C. Zhang, Combined Neyman-Pearson chi-square: An improved approximation to the Poisson-likelihood chi-square, Nucl. Instrum. Methods Phys. Res., Sect. A **961**, 163677 (2020).

[44] C. Andreopoulos *et al.*, The GENIE neutrino Monte Carlo generator, Nucl. Instrum. Methods Phys. Res., Sect. A **614**, 87 (2010).

[45] C. Andreopoulos, C. Barry, S. Dytman, H. Gallagher, T. Golan, R. Hatcher, G. Perdue, and J. Yarba, The GENIE neutrino Monte Carlo generator: Physics and user manual, arXiv:1510.05494.

[46] J. Allison *et al.*, Recent developments in GEANT4, Nucl. Instrum. Methods Phys. Res., Sect. A **835**, 186 (2016).

[47] J. Calcutt, C. Thorpe, K. Mahn, and L. Fields, GEANT4Reweight: A framework for evaluating and propagating hadronic interaction uncertainties in GEANT4, J. Instrum. **16**, P08042 (2021).

[48] B. P. Roe, Statistical errors in Monte Carlo estimates of systematic errors, Nucl. Instrum. Methods Phys. Res., Sect. A **570**, 159 (2007).

[49] P. Abratenko *et al.* (MicroBooNE Collaboration), Novel approach for evaluating detector-related uncertainties in a LArTPC using MicroBooNE data, arXiv:2111.03556.

[50] P. Abratenko *et al.* (MicroBooNE Collaboration), Measurement of space charge effects in the MicroBooNE LArTPC using cosmic muons, J. Instrum. **15**, P12037 (2020).

[51] C. Adams *et al.* (MicroBooNE Collaboration), A method to determine the electric field of liquid argon time projection chambers using a UV laser system and its application in MicroBooNE, J. Instrum. **15**, P07010 (2020).

[52] B. Efron and R. J. Tibshirani, *An Introduction to the Bootstrap*, Monographs on Statistics and Applied Probability No. 57 (Chapman & Hall/CRC, Boca Raton, Florida, USA, 1993).

[53] C. A. Argüelles, A. Schneider, and T. Yuan, A binned likelihood for stochastic models, J. High Energy Phys. 06 (2019) 030.

[54] T. Hauschild and M. Jentschel, Comparison of maximum likelihood estimation and chi-square statistics applied to counting experiments, Nucl. Instrum. Methods Phys. Res., Sect. A **457**, 384 (2001).

[55] M. L. Eaton, *Multivariate Statistics: A Vector Space Approach* (John Wiley and Sons, New York, 1983).

[56] See Supplemental Material at http://link.aps.org/supplemental/10.1103/PhysRevLett.128.151801 for validation of overall model, fake data studies, master equation of unfolding, tabulated values of cross section, and covariance matrices, which includes Refs. [57–76].

[57] S. Baker and R. D. Cousins, Clarification of the use of CHI square and likelihood functions in fits to histograms, Nucl. Instrum. Methods **221**, 437 (1984).
[58] J. Tena-Vidal *et al.* (GENIE Collaboration), Neutrino-nucleon cross-section model tuning in GENIE v3, Phys. Rev. D **104**, 072009 (2021).
[59] R. Carrasco and E. Oset, Interaction of real photons with nuclei from 100 to 500 MeV, Nucl. Phys. **A536**, 445 (1992).
[60] J. A. Nowak (MiniBooNE Collaboration), Four momentum transfer discrepancy in the charged current π^+ production in the MiniBooNE: Data vs theory, AIP Conf. Proc. **1189**, 243 (2009).
[61] K. S. Kuzmin, V. V. Lyubushkin, and V. A. Naumov, Lepton polarization in neutrino nucleon interactions, Mod. Phys. Lett. A **19**, 2815 (2004).
[62] C. Berger and L. M. Sehgal, Lepton mass effects in single pion production by neutrinos, Phys. Rev. D **76**, 113004 (2007).
[63] K. M. Graczyk and J. T. Sobczyk, Erratum: Form factors in the quark resonance model, Phys. Rev. D **79**, 079903(E) (2009).
[64] C. Berger and L. M. Sehgal, Partially conserved axial vector current and coherent pion production by low energy neutrinos, Phys. Rev. D **79**, 053003 (2009).
[65] D. Ashery, I. Navon, G. Azuelos, H. K. Walter, H. J. Pfeiffer, and F. W. Schlepütz, True absorption and scattering of pions on nuclei, Phys. Rev. C **23**, 2173 (1981).
[66] C. H. Llewellyn Smith, Neutrino reactions at accelerator energies, Phys. Rep. **3**, 261 (1972).
[67] J. Schwehr, D. Cherdack, and R. Gran, GENIE implementation of IFIC Valencia model for QE-like 2p2h neutrino-nucleus cross section, arXiv:1601.02038.
[68] K. M. Graczyk, D. Kielczewska, P. Przewlocki, and J. T. Sobczyk, C_5^A axial form factor from bubble chamber experiments, Phys. Rev. D **80**, 093001 (2009).
[69] J. Nieves, F. Sanchez, I. R. Simo, and M. J. Vicente Vacas, Neutrino energy reconstruction and the shape of the CCQE-like total cross section, Phys. Rev. D **85**, 113008 (2012).
[70] L. L. Salcedo, E. Oset, M. J. Vicente-Vacas, and C. Garcia-Recio, Computer simulation of inclusive pion nuclear reactions, Nucl. Phys. **A484**, 557 (1988).
[71] T. Leitner, L. Alvarez-Ruso, and U. Mosel, Charged current neutrino nucleus interactions at intermediate energies, Phys. Rev. C **73**, 065502 (2006).
[72] L. Tiator and S. Kamalov, Maid analysis techniques, in *Proceedings of the 5th International Workshop on the Physics of Excited Nucleons* (World Scientific, 2006), 10.1142/9789812773333_0002.
[73] T. Sjostrand, S. Mrenna, and P. Z. Skands, PYTHIA 6.4 physics and manual, J. High Energy Phys. 05 (2006) 026.
[74] T. Katori, Meson exchange current (MEC) Models in neutrino interaction generators, AIP Conf. Proc. **1663**, 030001 (2015).
[75] D. Rein and L. M. Sehgal, Neutrino-excitation of baryon resonances and single pion production, Ann. Phys. (N.Y.) **133**, 79 (1981).
[76] S. G. Mashnik, A. J. Sierk, K. K. Gudima, and M. I. Baznat, CEM03 and LAQGSM03—new modeling tools for nuclear applications, J. Phys. **41**, 340 (2006).
[77] T. Golan, J. T. Sobczyk, and J. Zmuda, NuWro: The Wroclaw Monte Carlo generator of neutrino interactions, Nucl. Phys. B Proc. Suppl. **229–232**, 499 (2012).
[78] Y. Hayato, A neutrino interaction simulation program library NEUT, Acta Phys. Pol. B **40**, 2477 (2009), https://www.actaphys.uj.edu.pl/R/40/9/2477/pdf
[79] O. Buss, T. Gaitanos, K. Gallmeister, H. van Hees, M. Kaskulov, O. Lalakulich, A. B. Larionov, T. Leitner, J. Weil, and U. Mosel, Transport-theoretical description of nuclear reactions, Phys. Rep. **512**, 1 (2012).
[80] K. Abe *et al.* (T2K Collaboration), Measurement of double-differential muon neutrino charged-current interactions on C_8H_8 without pions in the final state using the T2K off-axis beam, Phys. Rev. D **93**, 112012 (2016).